Original Article

Monte Carlo Calculation of Beam Quality and Phantom Scatter Corrections for Lithium Formate Electron Paramagnetic Resonance Dosimeter for High-energy Brachytherapy Dosimetry

Subhalaxmi Mishra, T. Palani Selvam

Bhabha Atomic Research Centre, Radiological Physics and Advisory Division, Health, Safety and Environment Group, Mumbai, Maharashtra, India

Abstract

Purpose: To investigate beam quality correction, K_{QQ0} (r) and phantom scatter correction, K_{phan} (r) for lithium formate dosimeter as a function of distance r along the transverse axis of the high-energy brachytherapy sources ^{60}Co, ^{137}Cs, ^{192}Ir and ^{169}Yb using the Monte Carlo-based EGSnrc code system. **Materials and Methods:** The brachytherapy sources investigated in this study are BEBIG High Dose Rate (HDR) ^{60}Co (model Co0.A86), ^{137}Cs (model RTR), HDR ^{192}Ir (model Microselectron) and HDR ^{169}Yb (model 4140). The solid phantom materials investigated are PMMA, polystyrene, solid water, virtual water, plastic water, RW1, RW3, A150 and WE210. **Result:** K_{QQ0} (r) is about unity and distance independent for ^{60}Co, ^{137}Cs and ^{192}Ir brachytherapy sources, whereas for the ^{169}Yb source, K_{QQ0} (r) increases gradually to about 4 % larger than unity at a distance of 15 cm along the transverse axis of the source. For ^{60}Co source, phantoms such as polystyrene, plastic water, solid water, virtual water, RW1, RW3 and WE210 are water-equivalent but PMMA and A150 phantoms show distance-dependent K_{phan} (r) values. For ^{137}Cs and ^{192}Ir sources, phantoms such as solid water, virtual water, RW1, RW3 and WE210 are water-equivalent. However, phantoms such as PMMA, plastic water, polystyrene and A150 showed distance-dependent K_{phan} (r) values, for these sources. For ^{169}Yb source, all the investigated phantoms show distance-dependent K_{phan} (r) values. **Conclusion:** K_{QQ0} (r) is about unity and distance independent for ^{60}Co, ^{137}Cs and ^{192}Ir brachytherapy sources. Phantoms such as solid water, virtual water, RW1, RW3 and WE210 are water-equivalent for ^{60}Co, ^{137}Cs and ^{192}Ir brachytherapy sources. For ^{169}Yb source, all the investigated phantoms show distance-dependent K_{phan} (r) values.

Keywords: Beam quality correction, brachytherapy, lithium formate, Monte Carlo, phantom scatter correction

Received on: 14-09-2016 **Review completed on: 28-12-2016** **Accepted on: 21-02-2017**

Introduction

Quantity of interest in brachytherapy dosimetry is absorbed dose to water in liquid water phantom. For measurement purposes, the precise and reproducible placement of detectors in water phantom is a challenge, so various detectors and solid phantoms are used which are probably not water equivalent. At the brachytherapy photon energies, a given solid phantom will alter the attenuation and scattering characteristics of photons as compared to the liquid water phantom. Hence, detector response changes with the type of the solid phantom and the distance from the source to the point of measurement in the phantom.

Selvam *et al.*[1] reported methodologies for calculating beam quality correction, K_{QQ0} (r), and phantom scatter correction K_{phan} (r), for different solid phantoms. Using these methodologies, the authors calculated the above corrections for various detector materials and solid phantoms at the ^{137}Cs energy.[1] In another study by Subhalaxmi and Selvam,[2] correction factors K_{QQ0} (r) and K_{phan} (r) were reported for various solid-state detectors for ^{60}Co and ^{192}Ir brachytherapy sources.

Recently, electron paramagnetic resonance (EPR) studies have shown that lithium formate monohydrate (hereafter

Access this article online

Quick Response Code:

Website: www.jmp.org.in

DOI: 10.4103/jmp.JMP_95_16

Address for correspondence: Subhalaxmi Mishra, Bhabha Atomic Research Centre, Radiological Physics and Advisory Division, Health, Safety and Environment Group, Mumbai - 400 094, Maharashtra, India.
E-mail: b.subwu@gmail.com

How to cite this article: Mishra S, Selvam TP. Monte carlo calculation of beam quality and phantom scatter corrections for lithium formate electron paramagnetic resonance dosimeter for high-energy brachytherapy dosimetry. J Med Phys 2017;42:72-9.

known as lithium formate) is a suitable practical dosimeter.[3-5] Lithium formate dosimeter has many advantages such as little signal fading at normal atmospheric conditions, no angular dependence and linear response over a wide range (0.1 Gy to 100 kGy). Effective atomic number of lithium formate is 7.3 compared to 7.4 for water and is 5–6 times as sensitive as alanine dosimeter.[6] Lithium formate dosimeter is often being used for the measurements around brachytherapy sources.[7-10]

The purpose of this study is to calculate $K_{QQ0}(r)$ and $K_{phan}(r)$ for lithium formate EPR dosimeter for high-energy brachytherapy sources ^{169}Yb, ^{192}Ir, ^{137}Cs, and ^{60}Co. This study also includes comparison of $K_{QQ0}(r)$ and $K_{phan}(r)$ values of lithium formate detector with the previously published values of other solid-state detectors such as diamond and LiF at ^{60}Co, ^{137}Cs, and ^{192}Ir energies.[1,2] Investigation of $K_{QQ0}(r)$ and $K_{phan}(r)$ values of $Li_2B_4O_7$ detector at ^{169}Yb energies is also included in the present study for comparison against lithium formate. The EGSnrc-based[11] user-codes DOSRZnrc and FLURZnrc[12] are used in the study.

It must be noted that $K_{phan}(r)$ values for different detectors as reported in our previously published studies[1,2] at ^{60}Co, ^{137}Cs, and ^{192}Ir energies were based on phantom dimensions of 40 cm diameter × 40 cm height, whereas in the present study involving lithium formate detector, the phantom dimensions involved are 160 cm diameter × 160 cm height for ^{60}Co, and 80 cm diameter × 80 cm height for ^{137}Cs, ^{192}Ir, and ^{169}Yb. This approach is consistent with the guidelines on phantom dimensions recommended in the report of AAPM and ESTRO.[13] Hence, we repeated the calculations of $K_{phan}(r)$ for diamond, $Li_2B_4O_7$, and LiF at ^{60}Co, ^{137}Cs, and ^{192}Ir energies for a meaningful comparison against lithium formate. It is found that phantom dimensions do not significantly affect the correction factors; hence, it is not discussed in this study.

Materials and Methods

Radioactive sources, dosimeter, and phantom materials

The brachytherapy sources investigated in this study are BEBIG high-dose rate (HDR) ^{60}Co (model Co0.A86),[14] ^{137}Cs (model RTR),[15] HDR ^{192}Ir (model MicroSelectron),[16] and HDR ^{169}Yb (model 4140).[17] The photon energy spectra of ^{169}Yb and ^{192}Ir needed for the Monte Carlo calculations were taken from literature.[17,18] For the ^{60}Co source, two gamma lines 1.17 MeV and 1.33 MeV were considered. For the ^{137}Cs source, a photon of energy 0.662 MeV was used. The solid phantom materials investigated are polymethylmethacrylate (PMMA), polystyrene, solid water, virtual water, plastic water, RW1, RW3, A150, and WE210. Table 1 presents the elemental composition, <Z/A> (electron density), and ρ (mass density) of the investigated phantom materials including water. The atomic composition and density details of RW1 and virtual water phantoms were taken from the published studies.[19,20] The data on the remaining phantoms were taken from a study by Seco and Evans.[21]

Beam quality and phantom scatter corrections

As described in the published study by Selvam *et al.*,[1] $K_{QQ0}(r)$ and $K_{phan}(r)$ can be calculated at a brachytherapy beam quality Q for solid-state detectors using the following relations:

$$k_{Q,Q0} = [D_{w,Q}(r)/D_{det,Q}(r)]/[D_{w,Q0}/D_{det,Q0}] \quad (1)$$

$$K_{phan}(r) = [D_{det,Q}(r)/D_{det,phan,Q}(r)] \quad (2)$$

Here, $D_{w,Q}(r)$ and $D_{det,Q}(r)$ are the absorbed dose to water and absorbed dose to detector in liquid water at a distance r along the transverse axis of the photon emitting brachytherapy source of beam quality Q, respectively. $D_{w,Q0}$ and $D_{det,Q0}$ are the absorbed dose to water and absorbed dose to detector in water at the reference beam quality Q_0 (realistic ^{60}Co teletherapy beam), respectively. $D_{det,phan,Q}(r)$ is the absorbed dose to detector in the solid phantom at r from the brachytherapy source of beam quality Q.

Monte Carlo calculations

The Monte Carlo calculations of absorbed dose to lithium formate in water and in solid-water phantoms were based on the FLURZnrc user code.[12] As described in the previously published studies,[1,2] the photon fluence spectrum was scored along the transverse axis of the source (r = 1–15 cm) in 0.5 mm high and 0.5 mm thick cylindrical shells. The fluence spectrum was converted to collision kerma to water and detector materials by the use of the mass energy-absorption coefficients of water and the detector, respectively.[22] In the calculation of the collision kerma to detector, no detector was present. We assumed that the presence of the detector did not affect the photon fluence spectrum and the collision kerma may be approximated to absorbed dose. To verify this, we carried out auxiliary simulations using the DOSRZnrc user code,[11] in which the detector was positioned at 1 and 15 cm along the transverse axis of the ^{60}Co source in the PMMA phantom. The values of the absorbed dose to detector obtained at 1 cm and 15 cm were compared with the values of the collision kerma of the detector (agreement was within 0.3%). This suggests that FLURZnrc user code can be used for calculating $K_{QQ0}(r)$ and $K_{phan}(r)$. Calculation of $D_{w,Q0}/D_{det,Q0}$ ratio is based on mass energy-absorption coefficients of water and detector material at 1.25 MeV, guided by the previously published studies.[1,2]

The values of the Monte Carlo parameters AE, AP, ECUT, PCUT, and ESAVE used in the FLURZnrc calculations were 0.521, 0.01, 0.01, 2, and 2 MeV, respectively. In the case of DOSRZnrc calculations, the value of ECUT used was 0.521 MeV (10 keV kinetic energy of electrons) and the values of other parameters were the same as that used in the FLURZnrc simulations. The parameters AE and AP were the low-energy thresholds for the production of knock-on electrons and secondary bremsstrahlung photons, respectively. The parameters ECUT and PCUT are electron and photon transport cutoff, respectively. ESAVE is a parameter related to the range rejection technique. Up to 10^9, photon histories were

Table 1: Elemental composition, electron density <Z/A> and mass density ρ of the investigated phantom materials

Element	Z	A	Water	Solid water	A150	WE210	RW3	RW1	Plastic water	Virtual water	PMMA	Polystyrene
Composition and mass fraction												
H	1	1.008	0.1119	0.081	0.1013	0.0821	0.0759	0.132	0.093	0.077	0.08054	0.07742
C	6	12.01		0.672	0.7755	0.6633	0.9041	0.794	0.6282	0.687	0.59985	0.92258
N	7	14.01		0.024	0.0351	0.0221			0.01	0.023		
O	8	15.99	0.8881	0.199	0.0523	0.2065		0.038	0.1794	0.189	0.31961	
F	9				0.0140		0.008					
Mg	12	24.31						0.009				
Cl	17	35.46		0.001		0.004		0.027	0.0096	0.001		
Ti	22											
Ca	20	40.08		0.023	0.1840	0.022	0.012		0.0795	0.023		
Br	35	79.9							0.0003			
Mass density (g/cm^3)			1	1.036	1.127	1.006	1.045	0.97	1.013	1.03	1.19	1.06
<Z/A>			0.555	0.54	0.547	0.540	0.536	0.565	0.545	0.538	0.539	0.538

PMMA: polymethylmethacrylate

simulated. The 1-σ statistical uncertainties on the calculated absorbed dose and collision kerma values were about 0.2%. The statistical uncertainties on the calculated values of $K_{QQ0}(r)$ and $K_{phan}(r)$ were <0.5%.

Results and Discussion

Beam quality correction, $K_{QQ0}(r)$

$K_{QQ0}(r)$ is about unity and distance independent for ^{60}Co, ^{137}Cs, and ^{192}Ir brachytherapy sources, whereas for the ^{169}Yb source, $K_{QQ0}(r)$ increases gradually to about 4% larger than unity for lithium formate dosimeter at a distance of 15 cm along the transverse axis of the source which is presented in Figure 1. When these results are compared with the published[1,2] values of other solid-state detectors such as diamond, LiF, and $Li_2B_4O_7$, it is observed that $K_{QQ0}(r)$ values of lithium formate are identical with the corresponding values of $Li_2B_4O_7$ detector at all distances for all the above sources. This is because of the fact that these two dosimeters have very similar dosimetric properties. For example, the effective atomic number and <Z/A> of lithium formate (7.23 and 0.514) are comparable to that of $Li_2B_4O_7$ (7.40 and 0.485) detector. The mass energy-absorption coefficient values of lithium formate $(\mu_{en}/\rho)_{LiFo}$ are only 6% higher to that of $(\mu_{en}/\rho)_{Li_2B_4O_7}$ in the energy range 10 keV to 1.5 MeV. Although the absolute values differ by 6%, $K_{QQ0}(r)$ values of these two detectors are identical, because $K_{QQ0}(r)$ is the ratio of absorbed dose to water and detector for a given beam quality normalized with the same ratio for the reference beam [Equation 1]. Hence, the ratio of absorbed dose to lithium formate and $Li_2B_4O_7$ at Q is equal to the same ratio at Q_0 which results in identical $K_{QQ0}(r)$ values for these two detectors.

$K_{QQ0}(r)$ values of diamond and LiF are also identical with that of lithium formate for ^{60}Co and ^{137}Cs brachytherapy sources. However, for ^{192}Ir and ^{169}Yb sources, diamond and LiF $K_{QQ0}(r)$ values are different from lithium formate detector (about 6% and 28% larger than unity at 15 cm for diamond detector for ^{192}Ir and ^{169}Yb, respectively).

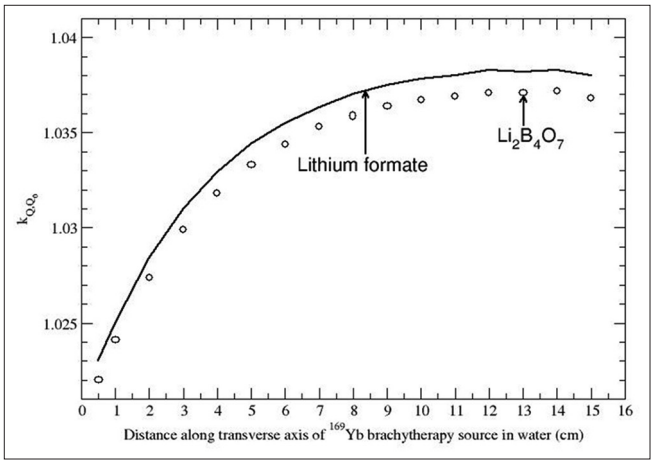

Figure 1: Beam quality correction, $K_{QQ0}(r)$, presented for lithium formate and $Li_2B_4O_7$ detectors as a function of distance along the transverse axis of the ^{169}Yb brachytherapy source.

Phantom scatter correction, $K_{phan}(r)$

The collision kerma to the detector at a distance r from the source in a phantom is due to both primary and scattered photons. The collision kerma due to primary photons is characterized by exponential attenuation of the primary photons and the mass energy-absorption coefficient (μ_{en}/ρ) of the detector at the primary photon energy. To understand the variations in the primary component of collision kerma, we analyzed the total linear attenuation coefficient (μ) data of photons in the energy range 10 keV–1.25 MeV for the investigated solid phantom materials and water using the state-of-the-art XCOM.[23] Table 2 presents the values of μ for all the phantom materials for photons in the range 10 keV–1.25 MeV. Table 3 presents ratio of μ values of the phantom materials normalized to water for the above energy range. It must be noted that the predominant primary gamma lines involved in the present study are 50 keV (^{169}Yb), 300 keV (^{192}Ir), 662 keV (^{137}Cs), and 1.25 MeV (^{60}Co). An analysis of exponential attenuation of

Table 2: Values of linear attenuation coefficient μ (cm^{-1}) presented for different phantom materials as a function of photon energy

Energy (MeV)	Water	Polystyrene	PMMA	A150	Plastic water	Solid water	Virtual water	RW1	RW3	WE210
0.01	5.3300	2.3521	3.9948	4.7199	10.7581	5.2929	5.2324	3.7801	3.5122	5.2362
0.02	0.8098	0.4626	0.6800	0.7969	1.6228	0.8517	0.8425	0.6464	0.6201	0.8391
0.03	0.3756	0.2798	0.3608	0.3924	0.6258	0.3936	0.3895	0.3286	0.3252	0.3858
0.04	0.2683	0.2314	0.2797	0.2887	0.3747	0.2773	0.2746	0.2473	0.2489	0.2709
0.05	0.2269	0.2105	0.2468	0.2477	0.2811	0.2323	0.2300	0.2148	0.2180	0.2265
0.06	0.2059	0.1982	0.2290	0.2263	0.2368	0.2094	0.2073	0.1976	0.2014	0.2039
0.08	0.1837	0.1829	0.2084	0.2032	0.1961	0.1857	0.1840	0.1785	0.1826	0.1807
0.10	0.1707	0.1721	0.1953	0.1893	0.1767	0.1722	0.1706	0.1668	0.1709	0.1675
0.15	0.1505	0.1535	0.1733	0.1674	0.1517	0.1516	0.1502	0.1477	0.1514	0.1474
0.20	0.1370	0.1401	0.1580	0.1525	0.1373	0.1380	0.1367	0.1347	0.1381	0.1341
0.30	0.1186	0.1216	0.1371	0.1322	0.1183	0.1195	0.1183	0.1168	0.1198	0.1161
0.40	0.1061	0.1089	0.1227	0.1182	0.1058	0.1069	0.1059	0.1046	0.1072	0.1039
0.50	0.0969	0.0994	0.1120	0.1080	0.0965	0.0975	0.0966	0.0954	0.0979	0.0948
0.60	0.0896	0.0919	0.1035	0.0998	0.0892	0.0902	0.0893	0.0883	0.0905	0.0877
0.80	0.0787	0.0807	0.0909	0.0876	0.0783	0.0792	0.0784	0.0775	0.0795	0.0770
1.00	0.0707	0.0726	0.0818	0.0788	0.0704	0.0712	0.0705	0.0697	0.0714	0.0692
1.25	0.0632	0.0649	0.0731	0.0705	0.0629	0.0637	0.0631	0.0623	0.0639	0.0619

PMMA: polymethylmethacrylate

Table 3: Values of linear attenuation coefficient μ (cm^{-1}) normalized to that of water presented for different phantom materials as a function of photon energy

Energy (MeV)	Polystyrene	PMMA	A150	Plastic water	Solid water	Virtual water	RW1	RW3	WE210
0.020	0.571	0.840	0.984	2.004	1.052	1.040	0.798	0.766	1.036
0.030	0.745	0.961	1.045	1.666	1.048	1.037	0.875	0.866	1.027
0.040	0.862	1.042	1.076	1.397	1.034	1.023	0.922	0.928	1.010
0.050	0.928	1.088	1.092	1.239	1.024	1.014	0.946	0.961	0.998
0.060	0.963	1.112	1.099	1.150	1.017	1.007	0.960	0.978	0.990
0.080	0.995	1.134	1.106	1.068	1.011	1.001	0.972	0.994	0.984
0.100	1.008	1.144	1.109	1.035	1.009	0.999	0.977	1.001	0.981
0.150	1.020	1.151	1.112	1.008	1.007	0.998	0.982	1.006	0.979
0.200	1.023	1.154	1.113	1.002	1.007	0.998	0.983	1.008	0.979
0.300	1.025	1.156	1.115	0.998	1.007	0.998	0.985	1.010	0.979
0.400	1.026	1.156	1.114	0.997	1.008	0.998	0.986	1.011	0.979
0.500	1.026	1.156	1.114	0.996	1.007	0.997	0.985	1.010	0.979
0.600	1.026	1.156	1.115	0.996	1.007	0.997	0.985	1.010	0.979
0.800	1.026	1.156	1.114	0.995	1.007	0.997	0.985	1.010	0.978
1.000	1.026	1.156	1.114	0.995	1.007	0.997	0.985	1.010	0.978
1.250	1.026	1.156	1.114	0.995	1.007	0.997	0.985	1.010	0.978

PMMA: polymethylmethacrylate

photons in water and the phantom materials suggests that for photon energy 50 keV and above, phantoms other than plastic water produce comparable attenuation at 1 cm. However, at 15 cm distance, the low-energy photons (below 50 keV) show significant variations in exponential attenuation by the phantom materials (other than WE210 at 50 keV) as compared to water. For photons of energies 300 keV and above, all the phantoms other than PMMA, A150, and WE210 demonstrate a comparable attenuation as compared to water (attenuation by polystyrene is larger by 5% at 300 keV as compared to water). The phantoms PMMA and A150 show higher attenuation than water. For example, for photon energy 1.25 MeV, PMMA and A150 phantoms demonstrate attenuation larger by factors of 1.16 and 1.11, respectively, at distance of 15 cm when compared to water. It can be noted that the above analysis of exponential attenuation of photons in the phantom materials has direct influence on the primary component of the collision kerma.

Quantification of collision kerma due to scattered photons is complex as it would depend on several factors such as fraction of photons that would undergo interactions such as photoelectric effect, Rayleigh scattering, Compton scattering, and pair production (for the photon energies investigated in the present study, pair production is not important). For example,

a photon with an initial energy hv_0 making a contribution at the detector location through Compton scattering depends on the following: (a) the spatial point in the phantom at which Compton scattering occurs, (b) probability that the scattered photon passes through the detector location which includes exponential attenuation of scattered photon energy between the scattering point and the detector, and (c) mass energy-absorption coefficient of the detector material at the scattered photon energy. μ values at both primary and scattered photon energies play an important role in the response of the detector.

The following discussion is based on an analysis of macroscopic cross section data of photons based on XCOM.[23] We restricted the analysis down to the photon energy of 30 keV, as a primary gamma line 50 keV of ^{169}Yb, after consecutive three Compton scatterings, each scattering through a polar angle of 180°, would result in a scattered photon energy of only about 30 keV. In this analysis, we normalized the macroscopic cross sections such as photoelectric and Compton to the total cross section. We did this normalization for all the phantom materials. The normalized Compton cross sections of all the phantoms are comparable to that of water at photon energies 150 keV and above. A similar analysis shows that A150, solid water, virtual water, and WE210 are comparable to that of water in the entire photon energy range of 50 keV–1.25 MeV, and RW1 and RW3 in the energy range of 80 keV–1.25 MeV. At low energies, the phantoms such as polystyrene, PMMA, A150, plastic water, RW1, and RW3 show significantly higher values of Compton cross sections. Figure 2 presents values of Compton macroscopic cross section normalized to total cross section for the investigated phantom materials in the photon energy range 30 keV–150 keV. At 30 keV, the normalized Compton cross section values are higher by factors of 1.40, 1.20, 1.08, 1.18, and 1.15, respectively, for the phantoms polystyrene, PMMA, A150, RW1, and RW3, when compared to that of water. For solid water, virtual water, and WE210, the factor is about 0.97. Due to the presence of high atomic number elements in the plastic water, the Compton cross section at 30 keV is significantly less as compared to water (factor is 0.6). At 50 keV, the above comparison provides a factor of 1.11 for polystyrene, 1.05–1.07 for PMMA, RW1, and RW3, 1.03 for A150, and 0.99 for solid water, WE210, and virtual water.

We have also analyzed the photoelectric cross section data of all the phantom materials. The photoelectric effect is important only at low photon energies. Hence, the comparison is restricted only in the energy range of 30–100 keV [Figure 3]. The analysis shows that the photoelectric cross sections are higher for phantom materials – plastic water, solid water, virtual water, and WE210. However, the photoelectric effect is important only for the ^{169}Yb source as its principal gamma line is at 50 keV (about 53% of total emission). At this energy, probability that the photon will undergo photoelectric effect is 0.12 for water and A150, 0.14 for solid water, virtual water, and WE210, about 0.10 for RW1 and RW3, and about 0.29 for plastic water. At 30 keV, the photoelectric effect is significant for all phantom materials. For example, the fractions of photons that will undergo photoelectric effect are 0.39 for water, 0.20 for polystyrene, 0.3 for PMMA, 0.37 for A150, 0.63 for plastic water, 0.42 for solid water, virtual water, and WE210, and 0.34 for RW1.

In the present study, Rayleigh scattering is important only at ^{169}Yb energies. At 30 keV, water, PMMA, and polystyrene show normalized Rayleigh cross section value of about 0.12; A150, solid water, virtual water, RW1, RW3, and WE210 show a value of about 0.10. At this energy, the normalized Rayleigh scattering cross section for plastic water is 0.08. At 50 keV, all phantoms show significantly smaller cross section than water (smaller by factor of 0.75–0.86 depending on the phantom).

In summary, the response of the detector material investigated in the present study is due to both primary and scattered photons. The primary component of the collision kerma dominates at short distances; hence, there is a tendency for

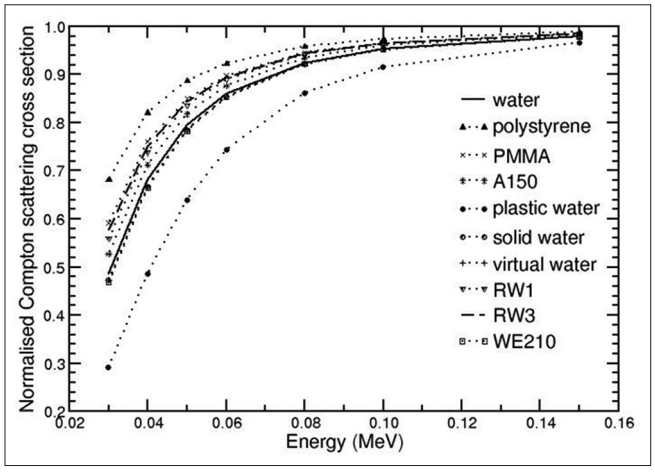

Figure 2: Macroscopic Compton cross section normalized to total macroscopic cross section as a function of photon energy. Data are based on XCOM.

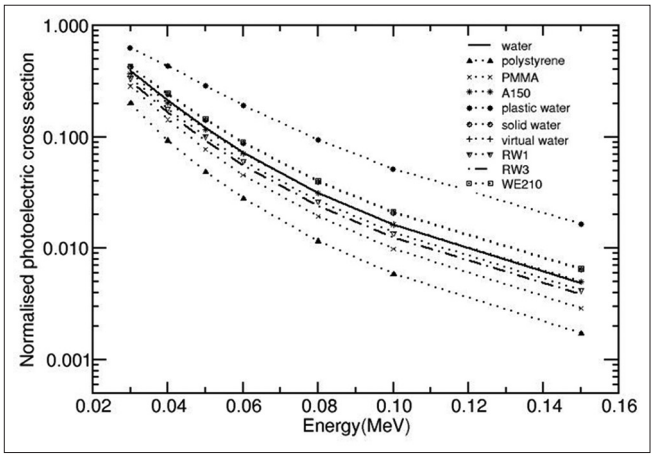

Figure 3: Macroscopic photoelectric cross section normalized to total macroscopic cross section as a function of photon energy. Data are based on XCOM.

all the phantom materials to be water equivalent at smaller distances. However, as the distance increases, the scatter contribution relative to primary is expected to increase as the primary component decreases due to inverse square fall in the primary photon fluence. Hence, depending on the photon source, the phantom materials having comparable values of μ (at both primary and scattered photon energies) and Compton scattering cross section with that of water are expected to be water equivalent.

It is observed that for a given source and for a given phantom, the detectors lithium formate and $Li_2B_4O_7$ exhibit similar trend of K_{phan} (r). Hence, in graphical presentations of K_{phan} (r), in addition to lithium formate, we included $Li_2B_4O_7$ data (see discussion).

^{60}Co source

For ^{60}Co source, the K_{phan} (r) values of diamond, LiF, and $Li_2B_4O_7$ detectors are identical to that of lithium formate detector for all the investigated phantom materials. Phantoms such as polystyrene, plastic water, solid water, virtual water, RW1, RW3, and WE210 are water equivalent (i.e., K_{phan} (r) is unity) at all distances (1–15 cm) for lithium formate detector. This is because for these phantom materials: (a) exponential attenuation of ^{60}Co photons at these distances are same, and (b) Compton cross section is comparable for wide range of photon energies (150 keV–1.25 MeV), whereas PMMA and A150 phantoms show increase in K_{phan} (r) values with distance, which are presented in Figure 4 (also included in this figure are results of $Li_2B_4O_7$). Although these phantoms have similar Compton cross section values as that of water (80 keV–1.25 MeV), differences in the exponential attenuation of primary photons [Tables 2 and 3 at 1.25 MeV] result in deviation of K_{phan} (r) values from unity (up to about 1.05 for PMMA and 1.04 for A150 at 15 cm) as the distance increases.

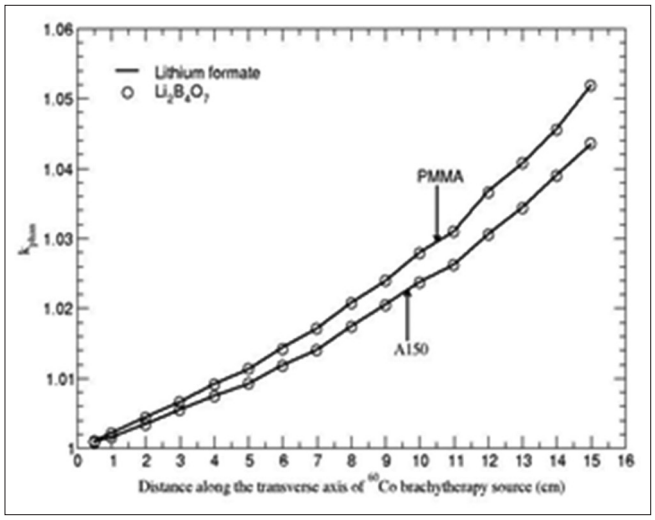

Figure 4: Phantom scatter correction, K_{phan} (r), presented for polymethylmethacrylate and A150 phantoms as a function of distance along the transverse axis of the ^{60}Co brachytherapy source for lithium formate and $Li_2B_4O_7$ detectors.

^{137}Cs brachytherapy source

Phantoms such as solid water, virtual water, RW1, RW3, and WE210 are water equivalent at all distances (1–15 cm) for lithium formate detector. Remaining phantoms such as polystyrene, plastic water, PMMA, and A150 show distance-dependent K_{phan} (r) values, which are presented in Figure 5. K_{phan} (r) decreases with r for polystyrene phantom which is due to increased contribution from multiple scattered photons. At low energy, polystyrene has high Compton scattering cross section than water. For plastic water, PMMA, and A150 phantom, K_{phan} (r) increases with r. Both PMMA and A150 phantoms have higher μ for a wide range of photon energies (40 keV–1.25 MeV). Hence, K_{phan} (r) increases with r. For plastic water, the scatter contribution is affected by: (a) higher values of μ at low-energy photons (40–100 keV), (b) smaller Compton scattering cross section at low-energy photons, and (c) higher values of photoelectric cross section at low-energy photons. K_{phan} (r) values of lithium formate are identical to that of $Li_2B_4O_7$ for all the phantom materials [Figure 5]. For A150 and plastic water phantoms, K_{phan} (r) values of diamond and LiF detectors are identical to that of lithium formate. However, for PMMA and polystyrene phantoms, the values differ with a maximum deviation of about 2% to that of lithium formate, which is not significant.

^{192}Ir brachytherapy source

Phantoms such as solid water, virtual water, RW1, RW3, and WE210 are water equivalent at all distances (1–15 cm) for lithium formate detector. Polystyrene, plastic water, PMMA, and A150 phantoms show distance-dependent K_{phan} (r) values, which are presented in Figure 6. K_{phan} (r) decreases with r (maximum up to 0.906 at 15 cm) in polystyrene phantom. Explanation given for ^{137}Cs is applicable for ^{192}Ir. However, degree of deviation of K_{phan} (r) values from unity is larger for ^{192}Ir because of increased photon scattering. For PMMA, A150, and plastic water phantoms, K_{phan} (r) increases with r. K_{phan} (r)

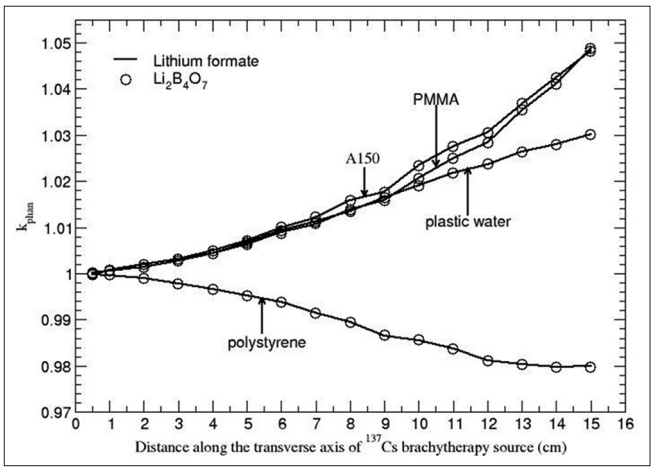

Figure 5: Phantom scatter correction, K_{phan} (r), presented for polymethylmethacrylate, polystyrene, plastic water, and A150 phantoms as a function of distance along the transverse axis of the ^{137}Cs brachytherapy source for lithium formate and $Li_2B_4O_7$ detectors.

increases to 1.026, 1.049, and 1.10 at a distance of 15 cm for PMMA, A150, and plastic water phantoms, respectively. $K_{phan}(r)$ values of lithium formate are identical to that of $Li_2B_4O_7$ for all the investigated phantom materials [Figure 6]. However, $K_{phan}(r)$ value is higher by about 3% for diamond detector and 3% smaller for LiF detector at a distance of 15 cm to that of lithium formate detector for PMMA and polystyrene phantoms.

^{169}Yb brachytherapy source

Distance-dependent $K_{phan}(r)$ values of lithium formate are presented in Figure 7 for all the investigated phantom materials. For a given r, phantoms such as solid water, virtual water, and WE210 show statistically identical values of $K_{phan}(r)$. This is because at ^{169}Yb energies, Compton is the predominant interaction and the cross section values of these phantoms are comparable. As the distance increases, $K_{phan}(r)$ increases to about 1.07 for these phantoms. Phantoms such as PMMA, polystyrene, RW1, and RW3 show decrease in $K_{phan}(r)$ values with r. However, RW1 and RW3 phantoms show a similar trend, as these two phantoms have comparable μ values and Compton cross section at the ^{169}Yb energies. For PMMA, $K_{phan}(r)$ decreases initially, from 0.988 to 0.901 when r is increased from 1 cm to 5 cm, and thereafter it is almost constant with a value of about 0.90. For PMMA, at ^{169}Yb energies, values of μ and Compton scattering cross section are higher when compared to water. It appears that scattering is a major contributor of $K_{phan}(r)$ than the exponential attenuation of primary photons for PMMA. Although values of μ and Compton scattering cross section for A150 phantom are comparable to that of PMMA, A150 shows a different trend in $K_{phan}(r)$ values. $K_{phan}(r)$ is constant (about 0.98) up to r = 6 cm and thereafter it increases to 1.06 at r = 15 cm. Thus, there is a tendency of compensation of exponential attenuation of primary photons by scatter contribution up to a distance of about 10 cm and thereafter exponential attenuation of primary photons is a major contributor of $K_{phan}(r)$. This is because density of PMMA (1.19 g/cm^3) is higher than A150 (1.127 g/cm^3) which results in more number of atoms present in PMMA than in A150. As a result, there will be more number of electrons present in PMMA than in A150 which enhances number of Compton scattering events comparatively more in PMMA.

For polystyrene, degree of decrease in $K_{phan}(r)$ with r is significant (about 36% smaller than unity at 15 cm). This is because for this phantom: (a) μ values at 50 keV are smaller than water, and (b) Compton scattering cross section is higher than water. The plastic water phantom shows increase in $K_{phan}(r)$ values with r. The degree of increase is significant for plastic water phantom (about 52% at a distance of 15 cm). This is because for this phantom at typical energy 50 keV of ^{169}Yb: (a) μ values are higher than water (factor is 1.24), (b) Compton scattering cross section is smaller than water (factor is 0.80), and (c) photoelectric cross section is higher by a factor of 2.34. $K_{phan}(r)$ values of diamond detector are higher by 6% and 11% for PMMA and polystyrene phantoms, respectively, to that of lithium formate detector at a distance of 15 cm, whereas for plastic water phantom, it is lower by 10% as compared to lithium formate detector. For LiF detector, $K_{phan}(r)$ values are lower by 4% and 7% for PMMA and polystyrene phantoms, respectively, to that of lithium formate detector. However, for plastic water phantom, it is higher by 9% as compared to lithium formate detector.

Effect of angular dependence on the correction factors

This work also includes the study of angular dependence effect on the correction factors. An auxiliary simulation was carried out, in which beam quality and phantom scatter corrections were obtained for different radial distances (r = 1, 2, 5, 10 cm) and polar angles (from 0° to 90° in an increment of 10°). The calculated data were normalized to the transverse axis data. The results showed that lithium formate and $Li_2B_4O_7$ did not show angular dependence for any of the investigated sources.

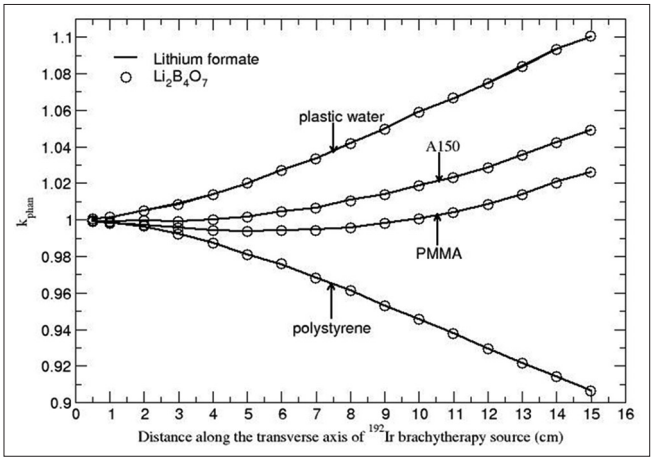

Figure 6: Phantom scatter correction, $K_{phan}(r)$, presented for polymethylmethacrylate, polystyrene, plastic water, and A150 phantoms as a function of distance along the transverse axis of the ^{192}Ir brachytherapy source for lithium formate and $Li_2B_4O_7$ detectors.

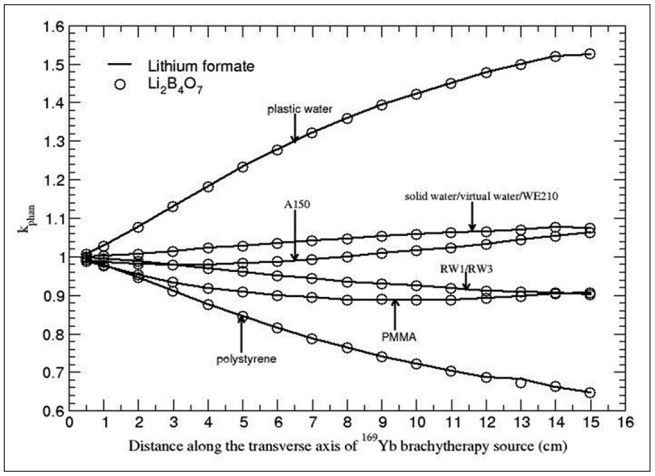

Figure 7: Phantom scatter correction, $K_{phan}(r)$, presented for lithium formate and $Li_2B_4O_7$ detectors as a function of distance along the transverse axis of the ^{169}Yb brachytherapy source for the investigated phantom materials.

Conclusions

Beam quality correction, $K_{QQ0}(r)$, and phantom scatter correction, $K_{phan}(r)$, for various solid phantoms were calculated for lithium formate detector as a function of distance along the transverse axis of the ^{60}Co, ^{137}Cs, ^{192}Ir, and ^{169}Yb brachytherapy sources using the Monte Carlo-based EGSnrc code system. $K_{QQ0}(r)$ is about unity and distance independent for ^{60}Co, ^{137}Cs, and ^{192}Ir brachytherapy sources, whereas for the ^{169}Yb source, $K_{QQ0}(r)$ increases gradually about 4% larger than unity.

For ^{60}Co source, phantoms such as polystyrene, plastic water, solid water, virtual water, RW1, RW3, and WE210 are water equivalent but PMMA and A150 phantoms show distance-dependent $K_{phan}(r)$ values for lithium formate detector. For ^{137}Cs and ^{192}Ir sources, phantoms such as solid water, virtual water, RW1, RW3, and WE210 are water equivalent but remaining phantoms such as PMMA, plastic water, polystyrene, and A150 show distance-dependent $K_{phan}(r)$ values. For ^{169}Yb source, all the investigated phantoms show distance-dependent $K_{phan}(r)$ values for lithium formate detector. $K_{QQ0}(r)$ and $K_{phan}(r)$ values of lithium formate detector are identical to the corresponding values of $Li_2B_4O_7$ for all the investigated sources. It is observed that as the energy of source increases, $K_{phan}(r)$ values of diamond, $Li_2B_4O_7$, LiF, and lithium formate are comparable.

Acknowledgment

The authors would like to thank Dr. Pradeepkumar K. S. Director, Health, Safety and Environment Group, Bhabha Atomic Research Centre (BARC) and Dr. D. Datta, Head, Radiological Physics and Advisory Division, BARC, for their encouragement and support throughout the study.

Financial support and sponsorship

Nil.

Conflicts of interest

There are no conflicts of interest.

References

1. Selvam TP, Mishra S, Vishwakarma RS. Monte Carlo calculation of beam quality correction for solid-state detectors and phantom scatter correction at ^{137}Cs energy. J Appl Clin Med Phys 2014;15:4445.
2. Subhalaxmi M, Selvam TP. Monte Carlo-based beam quality and phantom scatter corrections for solid-state detectors in ^{60}Co and 192Ir brachytherapy dosimetry. J Appl Clin Med Phys 2014;15:4907.
3. Vestad TA, Malinen E, Lund A, Hole EO, Sagstuen E. EPR dosimetric properties of formates. Appl Radiat Isot 2003;59:181-8.
4. Thomas JO, Tellgren R, Almlof J. Hydrogen bond studies: XCVL X-N map and ab initio MO-LCAO-SCF calculations of the difference electron density in non-centrosymmetric lithium formate monohydrate, LIHCOO: H2O. Acta Crystallogr 1975;31:1946-55.
5. Vestad TA, Gustafsson H, Lund A, Hole EO, Sagstuen E. Radiation-induced radicals in lithium formate monohydrate (LiHCO2:H2O). EPR and ENDOR studies of X-irradiated crystal and polycrystalline samples. Phys Chem Chem Phys 2004;6:3017-22.
6. Malinen E, Waldeland E, Hole EO, Sagstuen E. The energy dependence of lithium formate EPR dosimeters for clinical electron beams. Phys Med Biol 2007;52:4361-9.
7. Antonovic L, Gustafsson H, Carlsson GA, Carlsson Tedgren A. Evaluation of a lithium formate EPR dosimetry system for dose measurements around 192Ir brachytherapy sources. Med Phys 2009;36:2236-47.
8. Vanea ES, Levêque P, Abboud F, Bol A, Denis JM, Kolbun N, *et al.* Evaluation of the dose distribution gradient in the close vicinity of brachytherapy seeds using electron paramagnetic resonance imaging. Magn Reson Med 2009;61:1225-31.
9. Adolfsson E, Carlsson GA, Grindborg JE, Gustafsson H, Lund E, Carlsson Tedgren A. Response of lithium formate EPR dosimeters at photon energies relevant to the dosimetry of brachytherapy. Med Phys 2010;37:4946-59.
10. Waldeland E, Hole EO, Sagstuen E, Malinen E. The energy dependence of lithium formate and alanine EPR dosimeters for medium energy x rays. Med Phys 2010;37:3569-75.
11. Kawrakow I, Mainegra-Hing E, Rogers DW, Tessier F, Walters BR. The EGSnrc Code System: Monte Carlo Simulation of Electron and Photon Transport. NRCC Report PIRS-701. Ottawa, ON: National Research Council of Canada; 2010.
12. Rogers DW, Kawrakow I, Seuntjens JP, Walters BR, Mainegra-Hing E. NRC User Codes for EGSnrc. NRCC Report PIRS-702 (rev B). Ottawa, ON: National Research Council of Canada; 2010.
13. Perez-Calatayud J, Ballester F, Das RK, Dewerd LA, Ibbott GS, Meigooni AS, *et al.* Dose calculation for photon-emitting brachytherapy sources with average energy higher than 50 keV: Report of the AAPM and ESTRO. Med Phys 2012;39:2904-29.
14. Granero D, Pérez-Calatayud J, Ballester F. Technical note: Dosimetric study of a new Co-60 source used in brachytherapy. Med Phys 2007;34:3485-8.
15. Pérez-Calatayud J, Granero D, Ballester F, Casal E, Cases R, Agramunt S. Technical note: Monte Carlo derivation of TG-43 dosimetric parameters for radiation therapy resources and 3M ^{137}Cs sources. Med Phys 2005;32:2464-70.
16. Daskalov GM, Löffler E, Williamson JF. Monte Carlo-aided dosimetry of a new high dose-rate brachytherapy source. Med Phys 1998;25:2200-8.
17. Medich DC, Tries MA, Munro JJ 2nd. Monte Carlo characterization of an ytterbium-169 high dose rate brachytherapy source with analysis of statistical uncertainty. Med Phys 2006;33:163-72.
18. Shirley VS. Nuclear Data Sheets for A=192.Nuclear data sheet. Lawrence Berkeley laboratory, Berkeley, California.1991;64:205.
19. Reniers B, Verhaegen F, Vynckier S. The radial dose function of low-energy brachytherapy seeds in different solid phantoms: Comparison between calculations with the EGSnrc and MCNP4C Monte Carlo codes and measurements. Phys Med Biol 2004;49:1569-82.
20. Murphy MK, Piper RK, Greenwood LR, Mitch MG, Lamperti PJ, Seltzer SM, *et al.* Evaluation of the new cesium-131 seed for use in low-energy x-ray brachytherapy. Med Phys 2004;31:1529-38.
21. Seco J, Evans PM. Assessing the effect of electron density in photon dose calculations. Med Phys 2006;33:540-52.
22. Hubbell JH, Seltzer SM. Tables of X-ray Mass Attenuation Coefficients and Mass Energy-Absorption Coefficients, National Institute of Standards and Technology, Gaithersburg, MD; 1995. Available from: http://www.physics.nist.gov/PhysRefData/XrayMassCoef. [Last accessed on 2015 Dec 04].
23. Berger MJ, Hubbell JH, Seltzer SM, Chang J, Coursey JS, Sukumar R, *et al*. XCOM: Photon Cross Sections Database, National Institute of Standards and Technology; XCOM v3.1. Available from: http://www.nist.gov/pml/data/xcom/index.cfm. [Last accessed on 2013 Aug 01].